Appl Phys B (2012) 108:455–461
DOI 10.1007/s00340-012-4983-z

Applied Physics B
Lasers and Optics

Emission characteristics of Dy^{3+} ions in lead antimony borate glasses

M. Chandra Shekhar Reddy · B. Appa Rao · M.G. Brik · A. Prabhakar Reddy · P. Raghava Rao · C.K. Jayasankar · N. Veeraiah

Received: 13 October 2011 / Revised version: 29 January 2012 / Published online: 7 April 2012

Abstract Glasses with the composition $30PbO–25Sb_2O_3–(45-x)B_2O_3–xDy_2O_3$ for $x = 0$ to 1 were prepared in steps of 0.2 by the melt-quenching method. Various physical parameters, viz., density, molar volume, and oxygen packing density, were evaluated. Optical absorption and luminescence spectra of all the glasses were recorded at room temperature. From the observed absorption edges optical band gap, the Urbach energies are calculated; the optical band gap is found to decrease with the concentration of Dy_2O_3. The Judd–Ofelt theory was applied to characterize the absorption and luminescence spectra of Dy^{3+} ions in these glasses. Following the luminescence spectra, various radiative properties, like transition probability A, branching ratio β and the radiative life time τ for different emission levels of Dy^{3+} ions, have been evaluated. The radiative lifetime for the $^4F_{9/2}$ multiplet has also been evaluated from the recorded life time decay curves, and the quantum efficiencies were estimated for all the glasses. The quantum efficiency is found to increase with the concentration of Dy_2O_3.

M. Chandra Shekhar Reddy
Department of Physics, PRRM Engineering College, Shabad, Hyderabad 509 217, India

B. Appa Rao (✉) · A. Prabhakar Reddy
Department of Physics, Osmania University, Hyderabad 500 007, India
e-mail: apparao.bojja@gmail.com

M.G. Brik
Institute of Physics, University of Tartu, Riia 142, Tartu 51014, Estonia

P. Raghava Rao · N. Veeraiah
Dept. Physics, Acharya Nagarjuna University, Nuzvid Campus, Nuzvid 521201, A.P., India

C.K. Jayasankar
Department of Physics, S.V. University, Thirupathi 517 502, India

1 Introduction

Recently, the use of trivalent rare-earth ions in the development of field emission displays, plasma display panels, thin film electro-luminescent devices and white light emitting diodes has emerged as the principal motivation for extensive research in this field. Dy^{3+} is also one of the important rare-earth ions for the preparation of phosphors and also plays a major role in the production of white light luminescent materials. This ion is well known due to its IR emission transitions $^6H_{13/2} \rightarrow {}^6H_{15/2}$ (3.02 μm) and $^6H_{11/2} \rightarrow {}^6H_{13/2}$ (1.34 μm), which are considered as potential transitions for fiber amplifiers. Dy^{3+} ions exhibit two dominant emission bands in the blue region (470–500 nm) due to $^4F_{9/2} \rightarrow {}^6H_{15/2}$ transition and in the yellow region (560–600 nm) due to $^4F_{9/2} \rightarrow {}^6H_{13/2}$ transition. It is possible to achieve near white light emission by adjusting the yellow to blue intensity ratio value. Consequently, Dy^{3+}-activated luminescent materials attracted much attention [1–10] because of their significant applications as potential single-phase white phosphors.

Among various glass systems, heavy metal oxide-based glass systems like lead antimony oxide and borates find potential applications in non-linear optical devices (such as ultrafast optical triggers, optically poled materials, power limiters and broad band optical amplifiers operating around 1.5 μm) [11]. The antimony oxide-based glass materials are more stable against the pumping light and possess high refractive index and are transparent up to the far infrared wavelengths [12]. These factors favor antimony oxide-based

glasses to offer suitable environment for hosting the rare-earth ion like Dy^{3+} ion to give out high luminescence efficiency in the visible region. Antimony ions may also exist in the Sb^{5+} state (in addition to the Sb^{3+} state) and participate in the formation of a glass network with $Sb^{V}O_4$ structural units and likely to form the linkages with BO_4 structural units in $PbO–Sb_2O_3–B_2O_3$ glass network; such linkages are expected to influence the fluorescence efficiency of Dy^{3+} ions to a large extent. There are also reports suggesting that the Sb^{5+} ions participate in the glass network with SbO_6 (octahedral positions) structural units especially in the glasses mixed with rare-earth ions [13]. In the present investigation, we have attempted to investigate the fluorescence characteristics of Dy^{3+} ions incorporated into the lead antimony borate (LAB) glass system in the visible region. The study is further intended to evaluate the probabilities of principal luminescence transitions of Dy^{3+} ions in $PbO–Sb_2O_3–B_2O_3$ glass samples.

2 Experimental

For the present study, glasses of composition $30PbO–25Sb_2O_3–(45-x)B_2O_3–xDy_2O_3$ with $x = 0.2, 0.4, 0.6, 0.8, 1.0$ are chosen and samples are labeled as D_2, D_4, D_6, D_8 and D_{10}, respectively. Appropriate amounts of AR grade reagents of PbO, Sb_2O_3, B_2O_3, Dy_2O_3 powders are thoroughly mixed in agate mortar and melted in a silica crucible in the temperature range of 900 to 950 °C in a programmable electrical furnace for thirty minutes until bubble free liquid is formed. The resultant melt is poured in a brass mould and subsequently annealed at 250 °C for 2 h. The samples prepared were then ground and optical polished to the dimensions of 1 cm × 1 cm × 0.2 cm. Refractive index (n_d) of the samples was measured (at $\lambda = 589.3$ nm) using an Abbe refractometer with monobromo naphthalene as the contact layer between the glass and the refractometer prism. The optical absorption spectra of the samples were recorded at room temperature in the spectral wavelength range covering 300–2200 nm with a spectral resolution of 0.1 nm using JASCO Model V-670 UV-VIS-NIR spectrophotometer. The luminescence spectra and lifetime measurements were carried out at room temperature using JOBIN YVON Fluorolog-3 spectrofluorimeter using xenon arc lamp as radiation source. Infrared transmission spectra were recorded on a Bruker-FT IR-TENSOR27 spectrophotometer up to a resolution of 0.4 cm^{-1} in the spectral range 400–2000 cm^{-1} using potassium bromide pellets (300 mg) containing pulverized sample (1.5 mg).

3 Results

From the measured values of the density and average molecular weight M of the samples, various other physical parameters such as molar volume, oxygen packing density, Dy^{3+} ion concentration N_i, mean Dy^{3+} ion separation r_i, polaron radius r_p in $PbO–Sb_2O_3–B_2O_3:Dy_2O_3$ glass samples are computed using standard equations [14] and are presented in Table 1. Using the refractive index, various other optical parameters viz., molar refractivity (R_M), electronic polarizability (α_e) have also been evaluated and furnished in the same table. As the concentration of Dy^{3+} ions increased, a considerable increase in the density or a considerable decrease in the molar volume of samples is observed. Modification of the geometrical configurations of the glass network, change in coordination and the variation of dimensions of the interstitial holes can be considered to be responsible for such a variation of density. The oxygen packing density is also found to increase with the increase in the concentration of Dy^{3+} ions (Fig. 1). Such an increase indicates an increase in the structural compactness of the samples.

The infrared transmission spectra of $PbO–Sb_2O_3–B_2O_3:Dy_2O_3$ glasses (Fig. 2) exhibited three conventional bands originated from borate groups at 1330 cm^{-1} (due

Table 1 Various physical parameters of Dy^{3+} doped $PbO–Sb_2O_3–B_2O_3:Dy_2O_3$ glasses

Parameter	Glass				
	D_2	D_4	D_6	D_8	D_{10}
Density ρ (g/cm^3)	5.061	5.155	5.296	5.406	5.552
Molar volume V_m	33.94	33.44	32.66	32.11	31.38
Oxygen pack. density (g·atom/L)	70.71	71.77	73.48	74.74	76.48
Dy^{3+} ion conc. N_i ($\times 10^{21}$/cm^3)	0.11	0.22	0.33	0.45	0.58
Inter ionic distance R_i (Å)	20.87	16.57	14.47	13.05	11.99
Polaran radius r_p (Å)	8.41	6.68	5.83	5.26	4.83
Optical band gap E_o (eV)	3.44	3.43	3.42	3.40	3.37
Urbach energy ΔE (eV)	0.56	0.60	0.64	0.68	0.72
Refractive index (n)	1.59	1.59	1.59	1.59	1.59
Molar refraction (R_M)	11.39	11.27	11.04	10.87	10.65
Polarizability (α_e) ($\times 10^{-24}$) (cm^3)	4.51	4.47	4.37	4.31	4.22

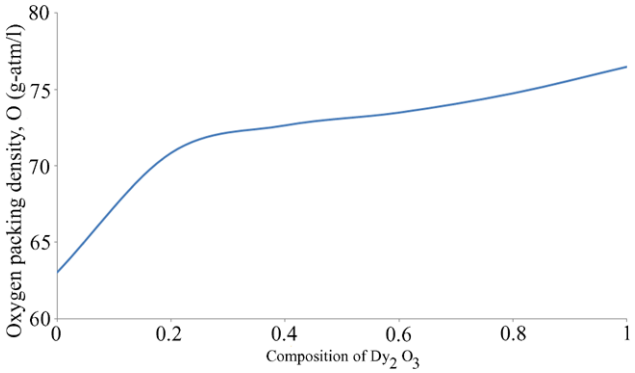

Fig. 1 Variation of oxygen packing density of $PbO–Sb_2O_3–B_2O_3–Dy_2O_3$ glasses doped with the concentration of Dy_2O_3

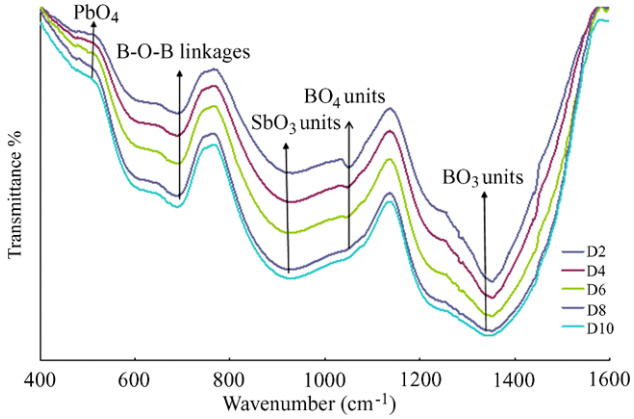

Fig. 2 FTIR spectra of $PbO–Sb_2O_3–B_2O_3:Dy_2O_3$

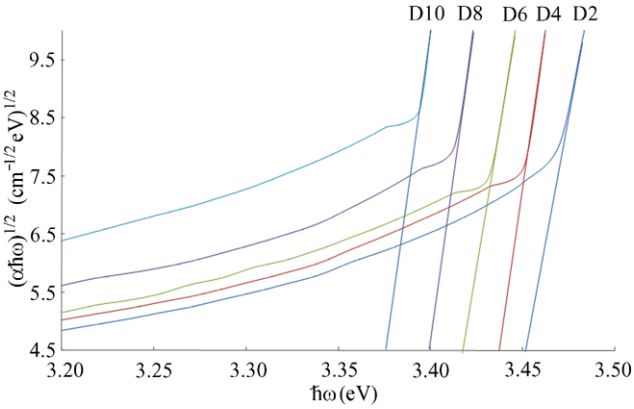

Fig. 3 Tauc plots for evaluation of optical band gap energy of $PbO–Sb_2O_3–B_2O_3$ glasses doped with Dy^{3+} ions

to BO_3 units), 1050 cm^{-1} (due to BO_4 units) and another band at 688 cm^{-1} due to bending vibrations of B–O–B linkages [15]. The ν_1 vibrational band of SbO_3 units appeared at 930 cm^{-1}. The ν_3 vibrational bands merged with the band due to bending vibrations of B–O–B linkages and may have formed a common vibrational band due to B–O–Sb linkages [16]. In addition, a band due to PbO_4 structural groups at about 462 cm^{-1} [17] is also observed in the spectra of all the samples. As the concentration of Dy^{3+} ions is increased in the glass network the intensity of the band due to BO_3 structural units is observed to increase at the expense of the band due to BO_4 units. Such an increase indicates that an increase in the degree of disorder in the glass network may be due to increasing modifying action of the Dy^{3+} ions.

The absorption edge observed at 376 nm for the glass D_2 is found to be spectrally shifted gradually towards higher wavelength with increase in the concentration of Dy_2O_3. From the absorption edges we have evaluated optical band gap for all these glasses by drawing Tauc plots (Fig. 3) between $(\alpha\hbar\omega)^{1/2}$ and $\hbar\omega$ as per the equation:

$$\alpha(\omega)\hbar\omega = c(\hbar\omega - E_o)^2 \quad (1)$$

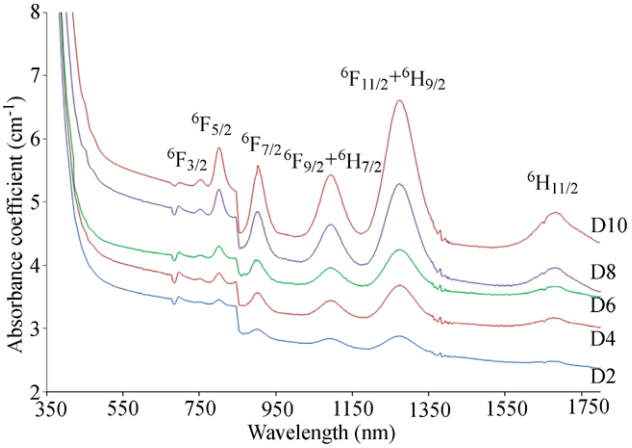

Fig. 4 Optical absorption spectra of $PbO–Sb_2O_3–B_2O_3$ glasses doped with Dy^{3+} recorded at room temperature. All transitions are from the ground state $^6H_{15/2}$

From the extrapolation of the linear portion of these curves, the values of optical band gap (E_o) obtained for $PbO–Sb_2O_3–B_2O_3:Dy_2O_3$ glasses and are presented in Table 1; the values of the Urbach energy (ΔE) were also calculated by taking the reciprocal of slopes of the linear part in the lower photon energy region of the curve and presented in Table 1. The optical band gap is found to decrease gradually with increase the concentration of Dy_2O_3. If Dy^{3+} ions participate in the depolymerization of the glass network similar to Pb^{2+} ions, more bonding defects and non-bridging oxygens (NBOs) may be created. Higher concentration of these ions in the glass network means higher numbers of donor centers are created; as a consequence, the degree of overlapping of the excited states of localized electrons with the empty 6f states on the neighboring sites increases, the impurity or polaron band becomes more extended into the main band gap. This new polaronic development might have shifted the absorption edge to the higher wavelength side (Table 1) or lead to shrinkage of the optical band gap with the increase in the concentration of Dy_2O_3.

The optical absorption spectra of Dy^{3+} doped $PbO–Sb_2O_3–B_2O_3$ glasses (Fig. 4) exhibited the following six well resolved peaks [18]:

$^6H_{15/2} \rightarrow {}^6H_{11/2}$ (1676 nm), $^6F_{11/2} + {}^6H_{9/2}$ (1270 nm), $^6F_{9/2} + {}^6H_{7/2}$ (1088 nm), $^6F_{7/2}$ (902 nm), $^6F_{5/2}$ (800 nm) and $^6F_{3/2}$ (751 nm)

The spectral intensities of these bands are found to increase with the content of Dy_2O_3; however, no significant shift in the position of the bands is observed.

The experimental oscillator strengths (OS) of the absorption transitions are estimated from the absorption spectra in

Table 2 Experimental ($f_{exp} \times 10^{-6}$) and calculated ($f_{cal} \times 10^{-6}$) spectral intensities of Dy^{3+} doped antimony lead borate glasses all the transitions are from the ground state $^6H_{15/2}$

Transition	Glass									
	D_2		D_4		D_6		D_8		D_{10}	
	f_{exp}	f_{cal}	f_{exp}	f_{cal}	f_{exp}	f_{cal}	f_{exp}	f_{cal}	f_{exp}	f_{cal}
$^6H_{11/2}$	0.533	0.542	0.387	0.716	1.172	0.629	0.7	0.49	0.913	1.249
$^6H_{9/2} + {}^6F_{11/2}$	3.286	3.634	2.632	4.441	5.821	3.281	3.624	2.626	4.429	5.817
$^6H_{7/2} + {}^6F_{9/2}$	1.342	1.56	1.201	1.964	2.364	1.357	1.596	1.195	1.989	2.39
$^6F_{7/2}$	1.185	1.399	0.883	1.752	2.305	1.141	1.285	0.915	1.682	2.22
$^6F_{5/2}$	0.555	0.587	0.551	0.888	1.077	0.547	0.605	0.418	0.81	1.122
$^6F_{3/2} + {}^6F_{1/2}$	0.119	0.095	0.074	0.12	0.181	0.103	0.114	0.079	0.153	0.212
r.m.s. deviation	±0.057		±0.115		±0.099		±0.1311		±0.0752	

terms of the area under an absorption peak. The numerical values of the OS are calculated using the following formula:

$$f = 4.319 \times 10^{-9} \int \varepsilon(\nu)\, d\nu \tag{2}$$

where $\varepsilon(\nu)$ is the molar absorptivity at frequency ν (this frequency is expressed in cm^{-1}) and is equal to $\frac{1}{LC}\log(I_0/I)$ with C being the rare-earth ion concentration (mol%), L the optical path length (thickness) and $\log(I_0/I)$ the optical density. The conventional Judd–Ofelt (JO) theory [19, 20] has been used to calculate the OS of the electric dipole transitions in the absorption spectra and estimate the radiative lifetimes of the emitting levels. The experimental and calculated OS are presented in Table 2.

The quality of fitting was determined in a standard way by the root mean squared deviation (RMS). The RMS values presented in Table 2 indicate a reasonably good fitting between theory and experiment demonstrating the applicability of JO theory.

The Judd–Ofelt parameters Ω_2, Ω_4 and Ω_6 were computed by the least square fitting analysis of the experimental oscillator strengths using matrix elements [18] and are presented in Table 3 along with the other pertinent data. The values of Ω_λ show the following order for all the three glasses: $\Omega_2 > \Omega_6 > \Omega_4$. The order of the Ω_λ parameters of Dy^{3+} ion in the studied glasses is well within the trends available in various other glass matrices [21, 22].

Figure 5 shows the emission spectra of dysprosium doped LAB glasses obtained with the excitation wavelength of 388 nm. The spectra exhibited the following emission bands:

$^4F_{9/2} \rightarrow {}^6H_{15/2}$ (484 nm), $^6H_{13/2}$ (576 nm), $^6H_{11/2}$ (666 nm) and $^4I_{15/2} \rightarrow {}^6H_{15/2}$ (455 nm)

The obtained JO intensity parameters were further employed to estimate the radiative transition probability $A_{JJ'}$ from the excited state $\langle f^N[\gamma, S, L]J|$ to the lower state $|f^N[\gamma', S', L']J'\rangle$. Summing up the $A_{JJ'}$ quantities over all possible final states, one can get the radiative life time τ of an excited energy level and the branching ratio $\beta_{JJ'}$ of the corresponding transition. The details of emission parameters for all the five Dy_2O_3 doped glasses are presented in Table 4. The fluorescence decay curves of $^4F_{9/2}$ multiplets of Dy^{3+} ion (Fig. 6) for all the glasses are observed to be single exponential.

Table 3 Judd–Ofelt intensity parameters ($\Omega_\lambda \times 10^{-20}$ cm^2) inantimony lead borate glasses doped with dysprosium ions in antimony

Sample	J–O intensity parameters ($\times 10^{-20}$ cm^2)		
	Ω_2	Ω_4	Ω_6
D_2	2.27	0.94	1.31
D_4	3.12	1.21	1.54
D_6	3.29	1.01	1.02
D_8	4.06	1.33	1.93
D_{10}	5.81	1.13	2.68

4 Discussion

Among the three constituents of $PbO–Sb_2O_3–B_2O_3$ glass system, Sb_2O_3 is an incipient glass network former and as such does not readily form the glass but does so in the presence of the modifier oxides like PbO and the glass former B_2O_3. Antimony oxide participates in the glass network with SbO_3 structural units with the oxygen at three corners and the lone pair of electrons of antimony at the fourth corner. The coordination polyhedra are joined by sharing the corners to form double infinite chains with the lone pairs pointing out from the chains. These chains are held together by weak secondary Sb–O bonds [23, 24]. It is also quite likely that a fraction of antimony ions exist in the Sb^{5+} state in these glasses because of the high melting temperature of the glass system. These Sb^{5+} ions participate in the

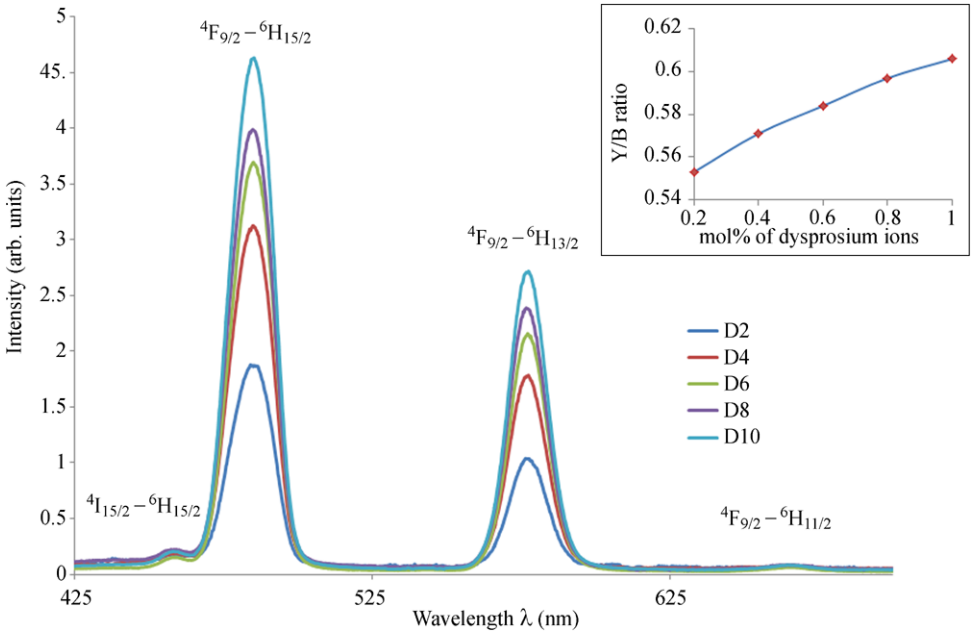

Fig. 5 Emission spectra of $PbO–Sb_2O_3–B_2O_3$ glasses doped with Dy^{3+} recorded at room temperature ($\lambda_{exc} = 388$ nm). The *inset* represents the variation of the Y/B ratio with the concentration of Dy^{3+} ions

Table 4 Radiative transition probability (A), total transition probability (A_T) radiative lifetime (τ_R) and branching ratio (β_R %) for the exited Dy^{3+} ions in lead antimony borate glasses

Transition	ν (cm^{-1})	D_2		D_4		D_6		D_8		D_{10}	
		A (s^{-1})	β_R(%)	A (s^{-1})	β_R(%)	A (s^{-1})	β_R(%)	A (s^{-1})	β_R(%)	A (s^{-1})	β_R(%)
$^4F_{9/2}$											
$\rightarrow {}^6H_{15/2}$	20661	99.2	21.7	102	20.7	130	23.2	132	19.2	138.1	16.8
$\rightarrow {}^6H_{113/2}$	17361	326.7	71.4	356.5	72.3	405.3	72.5	512	74.6	622.4	75.9
$\rightarrow {}^6H_{11/2}$	15015	31.6	6.9	34.1	6.9	23.9	4.27	42.5	6.19	59.6	7.26
		$A_T = 457.5$ (s^{-1}) $\tau_R = 2.19$ (ms)		$A_T = 492.6$ (s^{-1}) $\tau_R = 2.03$ (ms)		$A_T = 559.2$ (s^{-1}) $\tau_R = 1.79$ (ms)		$A_T = 686.5$ (s^{-1}) $\tau_R = 1.46$ (ms)		$A_T = 820.1$ (s^{-1}) $\tau_R = 1.22$ (ms)	
$^4I_{15/2}$											
$\rightarrow {}^6H_{15/2}$	21978	194.1	100	214.2	100	148.4	100	282.7	100	395.9	100
		$A_T = 194.1$ (s^{-1}) $\tau_R = 5.15$ (ms)		$A_T = 214.2$ (s^{-1}) $\tau_R = 4.67$ (ms)		$A_T = 148.4$ (s^{-1}) $\tau_R = 6.74$ (ms)		$A_T = 282.7$ (s^{-1}) $\tau_R = 3.54$ (ms)		$A_T = 395.9$ (s^{-1}) $\tau_R = 2.53$ (ms)	

glass network with Sb^VO_4 units and play a similar structural role to BO_4 units and may form cross linkages of the type Sb–O–B with the BO_4 units [25]. B_2O_3 is a network former and participates in the glass network with BO_3 and BO_4 structural units. PbO, when incorporated into the B_2O_3 glass network, normally converts sp^2 planar BO_3 structural clusters into more stable sp^3 tetrahedral BO_4 units. In general PbO participates in the glass network both with covalent and ionic bondings and participate in the glass network with $[PbO_{4/2}]$ pyramidal units connected in puckered layers.

The rare-earth ions that occupy different coordination sites with non-centro symmetric potential contribute significantly to Ω_2. Even with similar coordination, the differences in the distortion at these ion sites may lead to a distribution in the local crystal field. The variations in the sites with non–centro symmetric potential (that may arise due to the influences of the dielectric of media, the environment of the rare-earth ion and nephelauxetic effect) lead to changes in Ω_2 value. In fact, among the three J–O parameters, the parameter Ω_2 is related to the covalency and structural changes in the vicinity of the rare-earth ion (short-range effect) and Ω_4 and Ω_6 are related the long-range effects and are strongly influenced by the vibrational levels associated with the central rare-earth ions bound to the ligand atoms. The comparison of Ω_2 parameter for Dy^{3+} doped glasses shows a slightly increasing trend with the increase in the concentration of Dy_2O_3. According to the Judd–Ofelt theory, the Ω_λ parameters depend on crystal field parameter that determines the symmetry and distortion related to the structural change in the vicinity of Dy^{3+} ions. As the concentration of Dy^{3+} ions

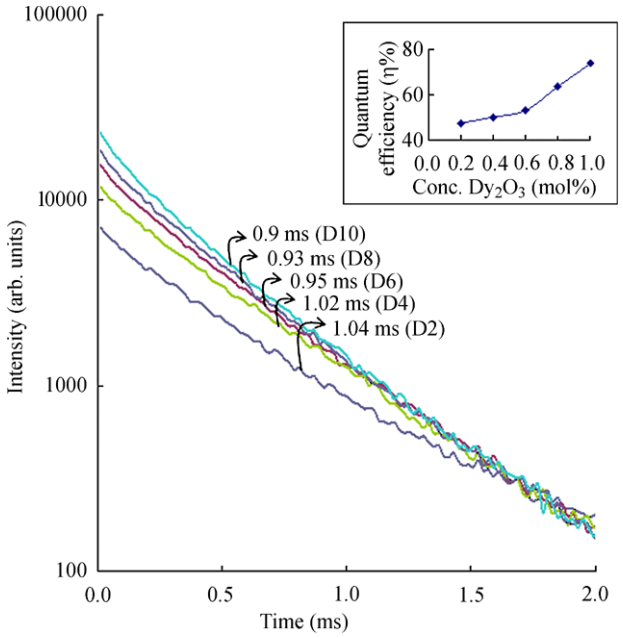

Fig. 6 Decay curve of $^4F_{9/2}$ level of Dy^{3+} ions in PbO–Sb_2O_3–B_2O_3 glasses. The *inset* represents the variation of quantum efficiency with the concentration of Dy_2O_3

increases, the average Dy–O distance will decrease. Such a decrease in the bond lengths produces stronger field around Dy^{3+} ions, leading to an increase in the value of Ω_2 with increase in the concentration of Dy_2O_3.

The increasing intensity or increasing quantum yield of the luminescence bands of Dy^{3+} ion in the glasses with increase in the concentration of Dy_2O_3 indicates that there is a decreasing cross relaxation i.e., the transfer of energy from the excited state of Dy ion by electric multipole interaction (more precisely dipole-dipole or dipole–quadrapole interactions) to neighboring Dy ion lying in the ground state. The examination of branching ratio β values of yellow emission (viz., $^4F_{9/2} \rightarrow {}^6H_{13/2}$), indicates an increasing trend with increase in the concentration of Dy_2O_3. Such a trend is probably because of a gradual decrease in the proportion of Sb^{5+} ions that participate in the glass network with Sb^{5+} structural units.

$^4F_{9/2} \rightarrow {}^6H_{15/2}$ and $^4F_{9/2} \rightarrow {}^6H_{13/2}$ occur in the blue (B) and yellow (Y) regions, respectively and intensities of these transitions depend on the Judd–Ofelt parameters Ω_2 and Ω_4 or in other words the integrated emission intensity ratio of these two transitions (Y/B ratio) is strongly influenced by site asymmetry (or structural changes in the vicinity of the Dy^{3+} ion) and covalency of the bonds with the ligand anions [21]. The value of this ratio shows an increasing trend with the increase in the concentration of Dy_2O_3, indicating increasing covalent environment for Dy^{3+} ions as shown in Fig. 5.

The parameter β_r (i.e., the branching ratio) of the luminescence transitions characterizes the lasing power of the potential laser transitions. The β_r values obtained for various luminescent transitions for Dy^{3+} ions indicate a gradual increase for the $^4F_{9/2} \rightarrow {}^6H_{13/2}$ yellow transition. It was well established that an emission level with β_r value nearly equal to 50 % is a potential laser emission [26]. Among various transitions, the transition $^4F_{9/2} \rightarrow {}^6H_{13/2}$ is found to have the highest values of β_r (>50 %) and this transition may therefore be considered as a possible laser transition.

The fluorescence lifetime τ_f of the $^4F_{9/2}$ multiplets evaluated from the decay profiles (Fig. 6) were found to be much lower than the radiative lifetime τ_r calculated by the Judd–Ofelt approach; see Table 4. In the weak excitation limit, the luminescence lifetime τ_f of the $^4F_{9/2}$ multiplet is given by

$$\tau_f = \frac{1}{A_{total}} = \frac{1}{A_r + A_{Ph} + A_{nret}} \tag{3}$$

where A_{total} is the total relaxation rate including the radiative transition rate A_r, the multi-phonon relaxation rate A_{ph}, and the non-radiative energy-transfer rate A_{nret}. The multi-phonon relaxation is inefficient owing to the significantly large energy gap between the $^4F_{9/2}$ emitting level and the next-lower level as compared with the maximum phonon energy of ~900 cm^{-1}. So only a radiative transition and non-radiative energy transfer relaxation are responsible for the depopulation of the $^4F_{9/2}$ multiplet. The reason for the large deviation between t_f and t_r is complex. On the one hand, the Judd–Ofelt theory is prone to overestimate the value of the radiative lifetime due to its partial inadequacy in predicting the radiative properties. Moreover, structural defects in the glass matrix may contribute $^4F_{9/2}$ level emission, leading to a t_f lower than expected.

The quantum yield (η) is defined as the radiative portion of the total relaxation rate of a given energy level [27]:

$$\eta = \frac{\tau_f}{\tau_r} \tag{4}$$

The value of η for the $^4F_{9/2}$ level of Dy^{3+} ions) determined for all the glasses and its variation with the concentration of Dy_2O_3 is represented as the inset of Fig. 6; the variation shows a decreasing trend of η with the concentration of Dy_2O_3. Such an increase is connected not only with the higher radiative relaxation probability but also with a reduction of the non-radiative transition probability. This is possibly due to the increase of low electron–phonon coupling of the Dy^{3+} ion with the high-energy phonons.

5 Conclusions

The optical absorption and photoluminescence spectra of Dy^{3+} ions in PbO–Sb_2O_3–B_2O_3 glasses have been studied. Oscillator strengths (OS) for various transitions have been

calculated using J–O theory. Good agreement between experimental and calculated OS has been achieved, demonstrating the applicability of JO theory. The radiative transition probabilities and branching ratios, evaluated for various luminescent transitions observed in the luminescence spectra, suggested the highest values (>50 %) for yellow emission (viz., $^4F_{9/2} \rightarrow {}^6H_{13/2}$) among various other transitions, indicating that it is a probable laser emission. The integrated emission intensity ratio of two transitions, viz., yellow ($^4F_{9/2} \rightarrow {}^6H_{13/2}$)/blue ($^4F_{9/2} \rightarrow {}^6H_{15/2}$) ratio, which is strongly influenced by site asymmetry or structural changes in the vicinity of the Dy^{3+} ion exhibited an increasing trend with the increase in the concentration of Dy_2O_3; from this observation we have concluded that there is an increasing covalent environment for Dy^{3+} ions with the ligand anions with increase in the concentration of Dy_2O_3 in the glass network. The variation of the quantum efficiency with the concentration of Dy_2O_3 exhibited an increasing trend; such an increase is attributed to the higher radiative relaxation probability.

Acknowledgements The author (B. Appa Rao) is thankful to Department of Science and Technology, Govt. India for supporting the work under OU-DST-PURSE program. M.G. Brik appreciates the support from the European Union through the European Regional Development Fund (Centre of Excellence "Mesosystems: Theory and Applications", TK114).

References

1. B.V. Ratnam, M. Jayasimhadri, K. Jang, H.S. Lee, J. Am. Ceram. Soc. **93**, 3857 (2010)
2. I.M. Nagpure, V.B. Pawade, S. Dhoble, J. Lumin. **25**, 9 (2010)
3. R. Martínez-Martínez, A.C. Lira, A. Speghini, C. Falcony, U. Caldiño, J. Alloys Compd. **509**, 3160 (2011)
4. L.H. Cheng, X.P. Li, J.S. Sun, H.Y. Zhong, Y. Tian, J. Wan, W.L. Lu, Y.F. Zheng, T.T. Yu, L.B. Huang, H.Q. Yu, B.J. Chen, Physica B **405**, 4457 (2010)
5. Y.N. Xue, F. Xiao, Q.Y. Zhang, Z.H. Jiang, J. Rare Earths **27**, 753 (2009)
6. Y. Fang, W.D. Zhuang, Y.S. Hu, X.W. Huang, J. Alloys Compd. **455**, 420 (2008)
7. K.N. Shinde, S.J. Dhoble, A. Kumar, J. Lumin. **131**, 931 (2011)
8. R. Zhang, X. Wang, J. Alloys Compd. **509**, 1197 (2011)
9. V.B. Rao, K.W. Jang, H.S. Lee, S.S. Yi, J.H. Jeong, J. Alloys Compd. **496**, 251 (2010)
10. K. Wei, D.P. Machewirth, J. Wenzel, E. Snitzer, G.H. Sigel, Opt. Lett. **19**, 904 (1994)
11. I.V. Kityk, A. Majchrowski, Opt. Mater. **25**, 33 (2004)
12. K. Terashima, T. Hashimoto, T. Uchino, S. Kim, T. Yoko, J. Ceram. Soc. Jpn. **104**, 1008 (1996)
13. Y. Hinatsu, H. Ebisawa, Y. Doi, J. Solid State Chem. **182**, 1694 (2009)
14. M.J. Weber, R. Cropp, J. Non-Cryst. Solids **4**, 137 (1981)
15. K.J. Rao, *Structural Chemistry of Glasses* (Elsevier, Amsterdam, 2002)
16. G. Srinivasarao, N. Veeraiah, J. Solid State Chem. **166**, 104 (2002)
17. T. Satyanarayana, I.V. Kityk, M. Piasecki, P. Bragiel, M.G. Brik, Y. Gandhi, N. Veeraiah, J. Phys., Condens. Matter **21**, 245104 (2009)
18. W.T. Carnall, P.R. Fields, K. Rajak, J. Chem. Phys. **49**, 4424 (1968)
19. B.R. Judd, Phys. Rev. **127**, 750 (1962)
20. G.S. Ofelt, J. Chem. Phys. **37**, 511 (1962)
21. P. Babu, C.K. Jayasankar, Physica B **279**, 262 (2009)
22. S. Surendra Babu, P. Babu, C.K. Jayasankar, W. Sievers, Th. Troster, G. Wortmann, J. Lumin. **126**, 109 (2007)
23. B. Dubois, J.J. Videau, J. Portier, J. Non-Cryst. Solids **88**, 355 (1986)
24. P.J. Miller, C.A. Cody, Spectrochim. Acta A **38**, 555 (1982)
25. D. Holland, A.C. Hannon, M.E. Smith, C.E. Johnson, M.F. Thomas, A.M. Beesley, Solid State NMR **26**, 172 (2004)
26. C. Hirayama, F.E. Camp, N.T. Melamid, K.B. Steinbruegge, J. Non-Cryst. Solids **6**, 342 (1971)
27. M. Rozanski, K. Wisniewski, J. Szatkowski, Cz. Koepke, M. Sroda, Opt. Mater. **31**, 548 (2009)